Transactions on Energy Systems and Engineering Applications

Article

Design of controller for dual input non-isolated DC/DC converter

Hamsavarthini Yoganandan[1,*] and Kanthalakshmi Srinivasan[1]

[1] Department of Electrical and Electronics Engineering, PSG College of Technology, Coimbatore, India.
[*] Correspondence: 1907re01@psgtech.ac.in

Received: 14 January 2024; Accepted: 14 January 2025; Published: 21 November 2025

Abstract: Renewable energy sources such as solar, battery, ultra-capacitor, wind, and fuel cell are used for the generation of electrical energy. However, these energy sources will have distinct electrical characteristics. To incorporate these multiple energy sources into a drive system, a power modulator is required to transmit and receive the energy from source to load and load to source. In the conventional method, energy from various sources is achieved from several single-input converters, essentially a power converter. However, it has drawbacks like design complexity, huge cost, bulky nature, and reduced efficiency. As a result, the concept of Dual Input DC-DC Converters (DICs) evolved to capture the interest of energy integration experts. In this study, a dual-input non-isolated DC/DC converter with reduced switches and diode configuration was considered, and an attempt was made to develop a closed-loop control of the converter. Further, the performance of the converter is evaluated in MATLAB/SIMULINK by considering its electrical parameters and time-domain specifications. From the results, the converter provides an average output power of 2560 W, an efficiency of 96%, and a high output voltage of 670 V during boost mode of operation. Along with that, the closed-loop configuration provides a reduced rise time of 15 ms and 3.29 ms, peak time of 21.8 ms and 8.5 ms, settling time of 65.29 ms and 70.75 ms, and a steady-state error of zero in both PI-Boost and PI-Buck mode operations.

1. Introduction

The population explosion and rapid industrial development have drastically increased the electricity demand worldwide. Conventional energy sources are inadequate to generate a power in order to match with the load requirements. These energy sources have severe negative impacts like non-renewable, pollution, etc. Generating and integrating the energy sources which has distinct V-I characteristics by using multiple single input converter was not efficient. As a result, dual input DC/DC converters are used as an alternative for multiple single input converters. A few isolated and non-isolated topologies of Dual Input Converter have been proposed in the literature and it was broadly classified as below.

How to cite this article: Hamsavarthini, Yoganandan; Kanthalakshmi, Srinivasan. Design of controller for dual input non-isolated DC/DC converter. *Transactions on Energy Systems and Engineering Applications*, 6(2): 604, 2025. DOI:10.32397/tesea.vol6.n2.604

There are three categories of converters based on the separation between the ports. The electrically connected converters use a DC link to connect the ports (Input and Output). Electromagnetically connected converter ports are isolated and it uses the DC link to connect the input and output ports. The magnetically connected converter was used to isolate the input port from the output port with the help of multiple winding transformers, but it adds design complexity and increases the system cost. Hence, a non-isolated dual input DC-DC converter was popularly used for renewable energy and hybrid electric vehicle applications.

A multi-input-single output DC-DC converter topology was proposed and their various operating states, small signal modeling, transfer function and performance comparison of the converter is verified both in simulation and experimentation [1]. The SEPIC, LUO, and interleaved LUO converters are compared in terms of converter output, motor parameters, and grid output. The performance of the converter is analyzed using several optimization techniques. From the result, the interleaved LUO converter performs better than the other two converters with a voltage gain ratio of 1:22, conversion efficiency of 98.3%, and grid current THD of 2.9% [2]. A simple power control strategy is proposed for steady-state and dynamic analysis of the converter. The performance analysis of the converter is made by comparing it with the existing topologies based on several criteria such as duty ratio and efficiency. Based on the results, the proposed converter features high voltage gain, low voltage stress, reduced part counts, with good efficiency [3].

A new multi-input non-isolated DC/DC converter with a high voltage transfer gain is proposed. The converter features a wide control range for various input powers with no restrictions on duty cycle, and less current stress. The proposed converter provides a good efficiency under various load conditions [4]. In order to integrate renewable energy sources (RES) with the load, a non-isolated multi-input DC-DC converter (MIC) topology is described. The proposed approach is validated through experimental results obtained using a laboratory prototype. Additionally, a 36 V/380 V, 200 W DC-DC converter's operating modes, characteristic waveforms, design specifications, simulation results, and experimental findings were presented [5]. A multiple-input DC/DC converter is studied in the MATLAB/Simulink environment and experimentally proven on a laboratory prototype using a dSPACE 1103 real-time digital controller [6].

Developed a H bridge cascade 5L-UPQC that maintains a constant DLCV during load variations, suppresses source current and load voltage harmonics, improves the shape of the current and voltage waveforms, and eliminates supply voltage oscillations (disturbance, sag, and swell). This study compares ANN, PIC, and SMC controllers for DLCV balancing, as well as other existing methods. The two test scenarios demonstrate that the developed method achieves significantly lower THD than previous approaches presented in the literature [7]. A Modified Dual Input DC-DC converter capable of integrating different V-I characteristic is proposed. The chosen converter was carefully examined on the experimental platform to validate simulation results. Experiments and simulations show that the converter's dynamic and steady state responses were satisfactory [8]. Two different kinds of dual-input buck-boost-type DC–DC converters (DIDC and BDIDC) to integrate hybrid energy sources for DC microgrid applications is proposed. To verify the simulation results, an experimental prototype is developed to validate the results. A simple control technique is used to ensure that the developed converter responds effectively in both steady-state and dynamic conditions [9].

A novel modified interleaved dual input – single output dc-dc converter that integrates the ultracapacitor and battery is proposed. Comparing the proposed converter to existing converters, it offers fewer components, a simpler construction, and increased efficiency [10]. The proposed converter is employed to integrate the energy sources from two sources individually or simultaneously. It provides a bidirectional capability in the Buck, Buck-Boost, and Boost modes. A MATLAB/Simulink is used to evaluate the proposed converter [11]. The proposed bridge type dual input DC-DC converters offer advantages such as reduced component count, compact construction, and efficient energy consumption over existing converter topologies. Two control techniques (ACM and OCC) to regulate output voltage at the desired value, and

compared their results. The transient study of the IBDC converter in the experimental platform revealed that the OCC technique outperforms the ACM method in terms of dynamic response [12].

A dual input, positive output voltage DC-DC converter system is presented. The feasibility of the converter is assessed through detailed analysis of all three modes of operation, including current and voltage stress analysis, the impact of ESR on voltage gain, power sharing, and power control strategies for voltage regulation during load and source side perturbations [13]. A multi-input buck-boost DC-DC converter is presented. The converter's analysis, design, simulation, and results from experiments prove that it's suitable for application like hybrid electric or renewable energy systems [14]. A double input converter topology capable of harvesting energy from various energy sources with varying voltage current characteristics is described. Simulation and experimental results indicate that the proposed converter is capable of integrating energy from many sources with varying characteristics, while also providing more source availability, flexibility, and control [15].

The investigation of various multi input DC-DC converter topologies indicates that there is no one topology capable of achieving all of the goals of cost, reliability, flexibility, efficiency, and modularity on its own. This paper discusses contemporary trends in the design of multi input and multi output DC-DC converters. The methods for synthesizing multi input converters, as well as their operational principles, advantages and disadvantages, are studied [16]. A new extendable multi-input step-up DC-DC converter (MISUC) topology is presented for efficiently connecting various energy sources with varying output characteristics to a common load. The operation and design of the MISUC are demonstrated in several modes, and design criteria are met to produce minimal output voltage ripple (OVR). Simulation and experimental findings were used to validate the converter's performance [17].

The use of a shunt active power filter (SHAPF) in conjunction with an Energy Storage System (ESS) and a Solar Energy System (SES) is proposed. The present effort attempts to achieve the following objectives, such as quick implementation to stabilize the voltage of the DC Link capacitor (DCLCV), harmonics mitigation and power factor improvement, which leads to satisfactory performance under load and solar power varying conditions [18]. A comparison of various multi-input DC/DC converter topologies based on battery life, soft-switching, source usage, and input-output isolation is presented. The review paper on multi-input DC/DC converters offers information and a selection guide for researchers, designers, and application engineers [19]. Based on input-output isolation, multi-input converters are classified into three types: magnetically connected, electromagnetically connected, and electrically connected converters. Each presented converter has some limitations. Future research aims to develop multi-input converters that are cost-effective, compact, and provide optimal control for both AC and DC output [20].

The operating waveforms and dynamic analysis of the proposed Dual input super boost DC-DC converter are thoroughly explored. The proposed converter's operation and performance in six modes are validated through simulation and experimental results [21]. A Quasi Z-Source Indirect Matrix Converter (QZSIMC) for PMG-based Direct Drive Wind Energy Conversion Systems (DDWECS) to improve voltage transfer ratio and manage output voltage under different loading situations is proposed. Two switching techniques were tested and compared using factors such as switching stress, shoot-through period, boost factor, and THD. The QZSIMC prefers the MSVPWM (modified space vector pulse-width modulation scheme) over the other option [22]. A prototype of a PEMFC/battery hybrid power supply system using the proposed Dual Input Super Boost Converter (DIBC) topology is developed to validate the theory and design. Experimental result shows ideal output characteristics and control effect of the developed prototype [23].

A novel technique for designing feedback controllers based on the Energy Factor concept is presented. This technique allows for multi-loop control of dc-dc boost converters and dc-dc buck-boost converters for off-grid PV applications. The proposed controller is executed in hardware for a 1.1 kW PV-array-fed

booster converter and it is validated by field test results and real-time weather information [24]. A two loop interleaved boost converter fed Permanent Magnet DC (PMDC) motor is proposed. The presented converter performance is assessed by using time domain parameters for three different speed ranges. The result shows that the simulation results are validated with the hardware outputs [25]. A new hybridized maximum power point tracking technique that combines an opposition-based reinforcement learning approach with a butterfly optimization algorithm has been proposed. The proposed methodology was evaluated on 6S, 3S2P, and 2S3P photovoltaic setups with varying shading circumstances. Experimental results reveal that the suggested strategy outperforms standard approaches in terms of adaptation while also mitigating load variation convergence and frequent exploration and exploitation patterns [26].

A mismatch loss mitigation algorithm is applied for DIDO converter. The proposed system's performance is simulated under five different shading patterns using MATLAB/Simulink, and the resulting PV curves were presented and it is also validated using a 200-watt PV system [27]. The remainder of this paper was organized as follows: Section 2 presents the circuit diagram, output equation, design parameters and steady-state waveform of the converter along with that an open and closed-loop simulation was analyzed under different operating modes of the converter. Performance evaluation followed by result and discussion are explained in Section 3. The conclusion for the converter topology was drawn in Section 4.

Research Significance

The DC-DC converters are essential electronic circuits that play a crucial role in modern industrial and commercial electronics. Understanding the different types of DC-to-DC converters and their respective functionalities is key to optimizes its efficiency and stability. There are several types of DC-DC converters, each with unique circuit topologies and characteristics. These topologies can be broadly categorized into two groups: non-isolated and isolated converters. Many Researchers have considered isolated and non-isolated converters and few have made a detailed analysis of the converters in different operating modes and their stability analysis. Only a very few researchers have considered non-isolated DC-DC converters with multiple input configurations. However, their performance is not analyzed in detail with electrical parameters and time domain specifications. To plug this gap, the electrical and time domain parameters are considered for performance analysis of the DC-DC converter both in open loop and closed loop configuration which in turn would result in achieving the improved efficiency, high average output power and output voltage, reduced time and improved speed of response of the converter.

2. Dual input DC/DC converter

The DIC comprises of two input sources, two power switches with anti-parallel diode and two power switches without anti-parallel diode, an inductor, capacitor, and resistive load and it was shown in Figure 1.

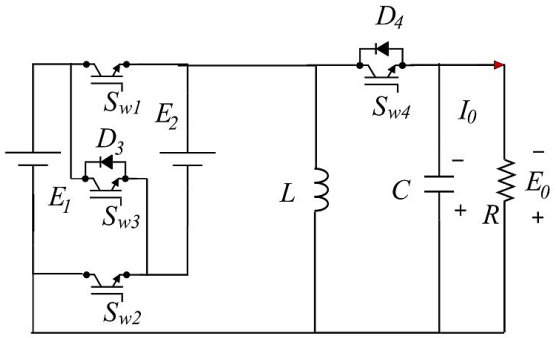

Figure 1. Circuit diagram of dual input DC/DC converter.

The basic working of dual input DC/DC Converter was similar to conventional single input DC/DC converter. Here the passive elements (L, C) charges the load for particular time period and it discharges for remaining time period. The power can be transmitted/received to and from source/load either concurrently or individually. Any one of the switches and the diode (SW1, SW2, SW3, and diode D4) will be in conduction for a particular period (unidirectional). During Bidirectional mode (SW4 and D3) will be in conduction. The power flow through the converter was controlled by adjusting the duty ratios of the corresponding switches.

2.1. Operating Modes, design parameters, analytical waveforms and simulation results of dual input DC-DC Converter

2.1.1. Source to load operation (State 1-4)

- **State 1** In this state, switch S_{W1} was ON. Source 1 delivers the energy to the inductor. However, the diode D_4, switches S_{W2} and S_{W3} are in a non-dynamic state as shown in Figure 2(a).
- **State 2** In this state of operation, the switch S_{W3} was turned ON. It is observed that the switch S_{W3} conduction makes a series combination of both input sources. Hence, the energy was transferred to the inductor from both the input sources simultaneously. The utilization of independent as well as simultaneous input sources are considered as a potential merit of this converter. This unique operation of the converter finds its applications like a hybrid EV, renewable energy, etc. In this state, switches S_{W1}, S_{W2}, and diode D_4 are in the non-dynamic state as shown in Figure 2(b).
- **State 3** Consider the switch S_{W2} was ON and other switches are in OFF state. In this state, Source 2 delivers the energy to the inductor as shown in Figure 2(c).
- **State 4** In this state, the switches S_{W1}, S_{W2}, and S_{W3} are in OFF state, and forward biases the diode D_4. The stored energy in the inductor L is transferred to the load as shown in Figure 2(d).

2.1.2. Load to source operation (State 5-6)

- **State 5** When the load has power during braking operation, the switch S_{W4} was turned ON and it charges the inductor L. Due to this, a $-E_0$ voltage was produced across the inductor as shown in Figure 2(e).
- **State 6** In this state, the switch S_{W4} was turned OFF. The inductor's stored energy was transferred to the input sources with the help of diode D_3. The voltage over the inductor is $E_1 + E_2$ as shown in Figure 2(f).

According to the volt-second balance equation, the average voltage of the inductor should be zero when the system is in a steady state. Equation (1) provides the inductor's average voltage over a cycle.

$$\int_0^{T_s} E_L \, dt = 0, \tag{1}$$

$$E_1 t_1 + (E_1 + E_2) t_3 + E_2 t_2 - E_C t_4 = 0, \tag{2}$$

where $t_1 = d_1 T_s$, $t_2 = d_2 T_s$, and $t_3 = d_3 T_s$. Dividing eq. (2) by T_s and substituting $E_C = -E_0$, we get:

$$E_1 d_1 + (E_1 + E_2) d_3 + E_2 d_2 + E_0 (1 - (d_1 + d_2 + d_3)) = 0. \tag{3}$$

The output voltage equation of the converter (when power flows from source to load side) is:

$$E_0 = -\left(\frac{E_1 d_1 + (E_1 + E_2) d_3 + E_2 d_2}{1 - (d_1 + d_2 + d_3)} \right). \tag{4}$$

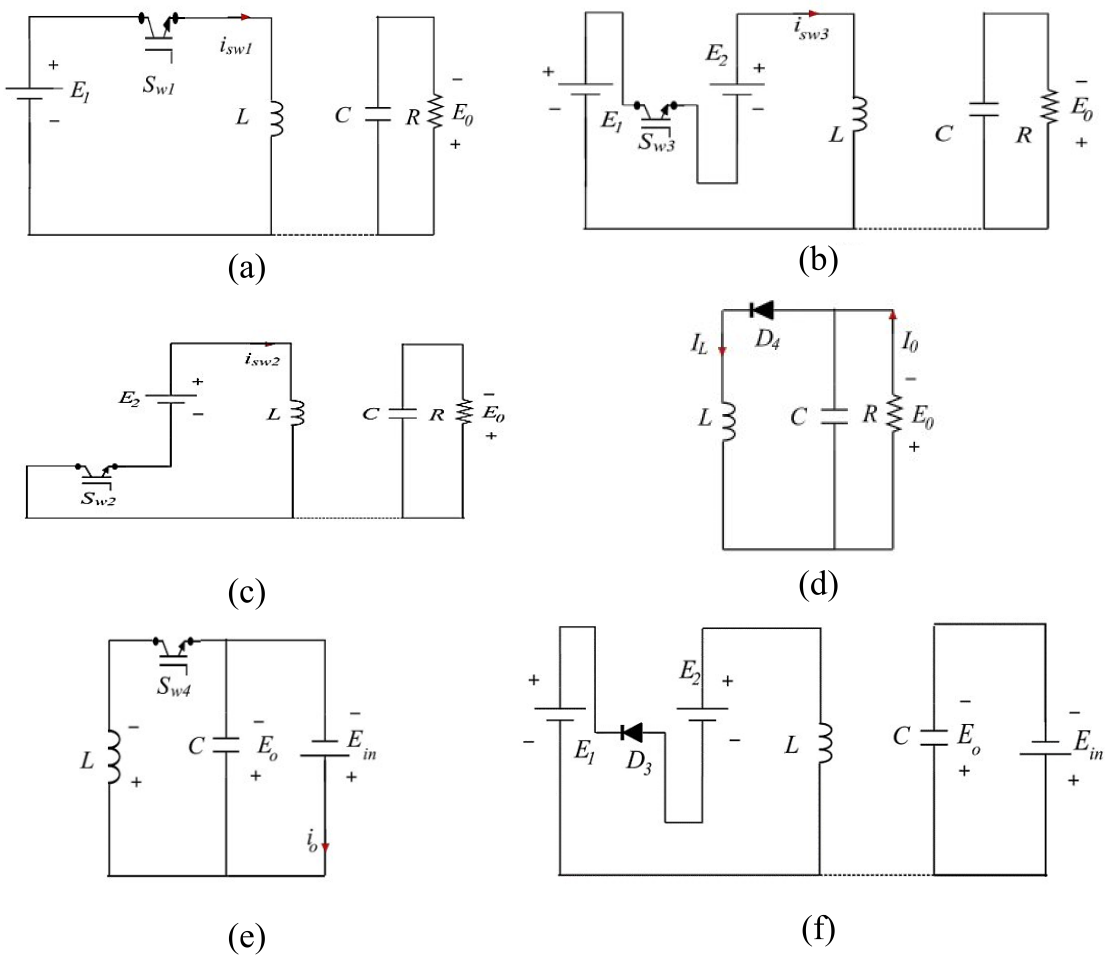

Figure 2. Mode of operation. (a) State 1. (b) State 2. (c) State 3. (d) State 4. (e) State 5. (f) State 6.

The average inductor voltage is given by:

$$\int_0^{T_s} E_L \, dt = 0, \tag{5}$$

$$E_C t_1 - (E_1 + E_2) t_2 = 0, \tag{6}$$

where $t_1 = d_4 T_s$, $t_2 = (1 - d_4) T_s$, and $E_C = -E_0$. Dividing eq. (6) by T_s and substituting $E_C = -E_0$,

$$-E_0 d_4 - (E_1 + E_2)(1 - d_4) = 0. \tag{7}$$

Output voltage equation of the converter (when power flows from load to source side):

$$(E_1 + E_2) = \frac{d_4}{1 - d_4}(-E_0). \tag{8}$$

2.1.3. Design parameters

The parameters considered for the converter under buck and boost mode are shown in Table 1.

Table 1. Simulation Parameters

S. No	Electrical Parameters	Specifications during	
		Boost Mode	**Buck Mode**
1	Voltage - E_1	48 V	
2	Voltage - E_2	36 V	
3	Duty ratio (d_1)	20%	15%
4	Duty ratio (d_3)	32.5%	10%
5	Duty ratio (d_2)	20%	15%
6	Inductor (L)	6.5 mH	
7	Capacitor (C)	433 μF	
8	Switching Frequency (F_s)	10 kHz	
9	Load Resistance (R)	10 Ω	
10	Output Voltage (E_o)	-160 V	-35 V

2.1.4. Analytical waveforms of the converter

Steady state waveform of the converter under continuous conduction mode (CCM) for source to load and load to source was shown in Figures 3 and 4.

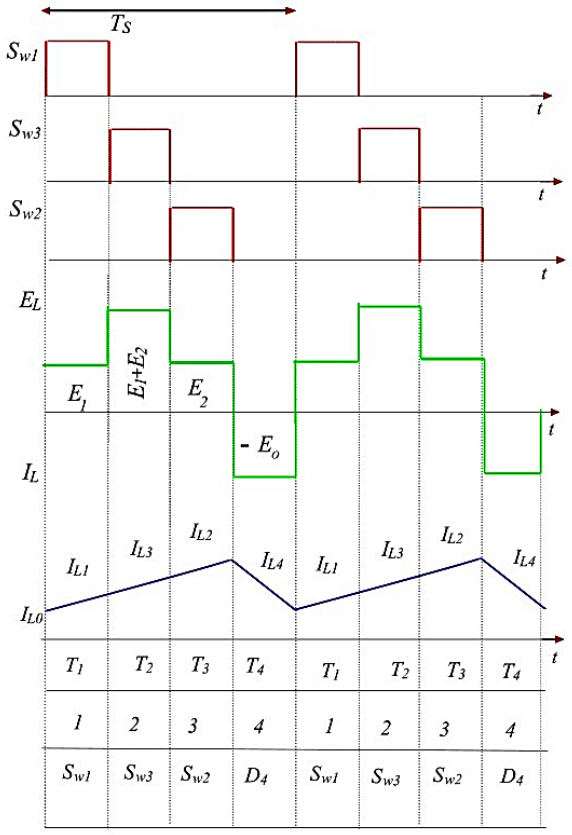

Figure 3. Source to Load waveform.

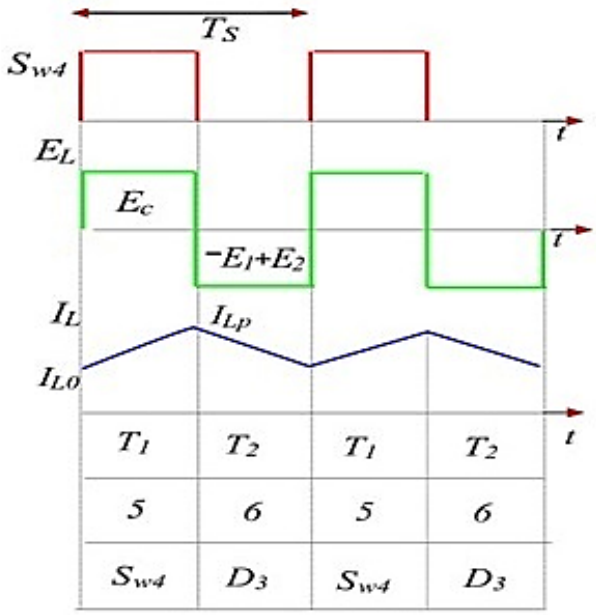

Figure 4. Load to Source waveform.

2.2. Simulation Results

The open and closed loop simulation was performed by considering the optimum behavior of various components in a dual input DC/DC converter.

2.2.1. Open loop simulation

The insulated-gate bipolar transistors were used as power switches. The boost and buck mode specification for various electrical parameters are given in Table 1. Output voltage of -160 V was obtained from boost mode with a duty ratio of $d_1 = 20\%$, $d_2 = 20\%$, and $d_3 = 32.5\%$ (To check the utility of the converter, output voltage is chosen as -160 V). The converter's output voltage during buck mode was -35 V, if the duty ratio were chosen as $d_1 = 15\%$, $d_2 = 15\%$, and $d_3 = 10\%$. The open loop schematic diagram of the dual input non-isolated DC/DC converter is shown in Fig. 5.

2.2.1.1. Boost Mode

In boost mode, the input voltages E_1, E_2 and the duty cycle provided to the switches S_{W1}, S_{W2}, and S_{W3} are shown in Table 1. Switch (S_{W1}) was assigned with the duty cycle (d_1), and the inductor was charged to 48 V (i.e., $E_1 - E_o$). The voltage across the inductor will be (i.e., $E_1 + E_2 - E_o$), i.e., 84 V, when the d_3 is applied to switch (S_{W3}).

Moreover, when d_2 is applied to the switch (S_{W2}), the inductor voltage will be 36 V (i.e., $E_2 - E_o$), and the inductor was finally discharged to a value of -158.5 V (i.e., $-E_o$). As shown in Fig. 6(a) and Fig. 6(b), the current flowing through the inductor was 57.63 A during charging and 57 A when it was discharging. The voltage across load resistance is -158.5 V (i.e., $-E_o$) and the current through the load resistance (-I_o) was -15.85 A, as shown in Fig. 6(c) and Fig. 6(d).

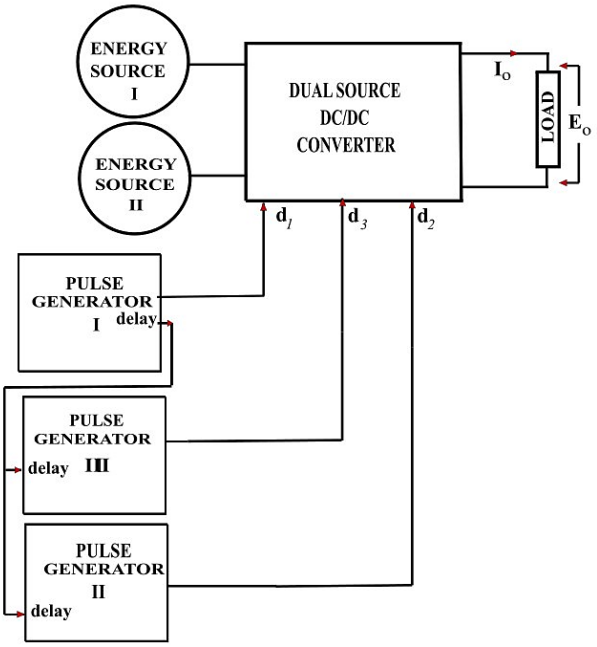

Figure 5. Open loop schematic of dual input DC/DC Converter.

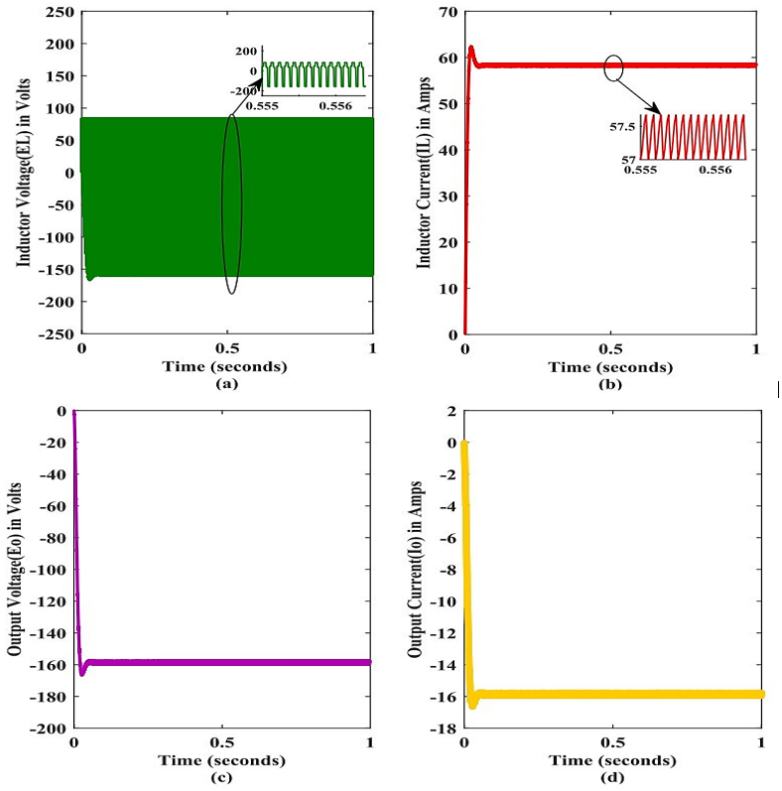

Figure 6. (a)Voltage across the inductor (b) Current through the inductor (c) Output voltage across the load (d) Output current through the load during boost mode.

2.2.1.2. Buck Mode

In buck mode, the input voltages E_1, E_2 and the duty cycle provided to the switches S_{W1}, S_{W2}, and S_{W3} are shown in Table 1. For duty cycle (d_1), the inductor charges to a voltage of 48 V (i.e., $E_1 - E_o$), for a duty cycle (d_2), the inductor charges to a voltage of 36 V (i.e., $E_2 - E_o$), and for duty cycle (d_3), the voltage across the inductor will be 84 V (i.e., $E_1 + E_2 - E_o$).

Later, the inductor voltage was -34.65 V (i.e., $-E_o$). The current through the inductor while charging and discharging will be from 5.79 A to 5.48 A, as shown in Fig. 7(a) and Fig. 7(b). The output voltage ($-E_o$) was -34.65 V, and the output current ($-I_o$) was -3.465 A across the load resistance, as shown in Fig. 7(c) and Fig. 7(d).

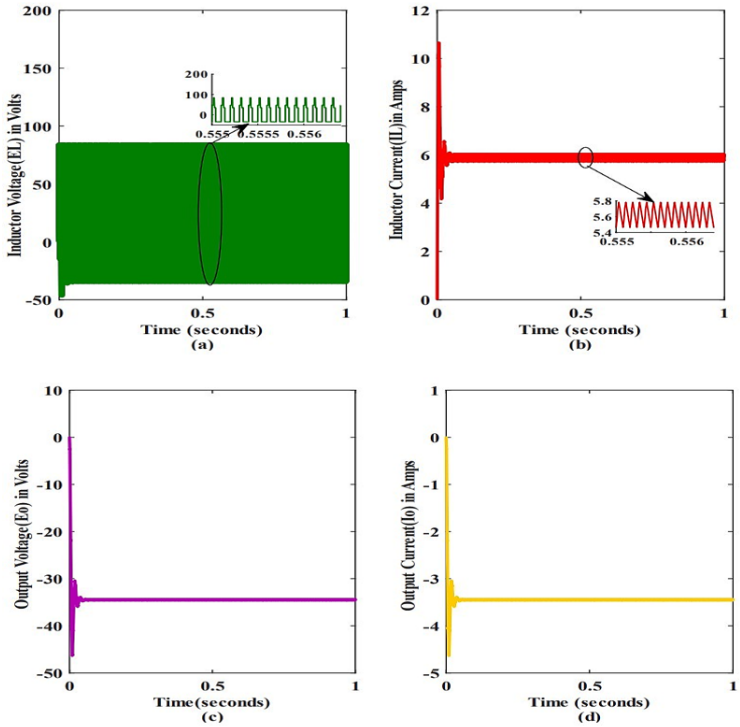

Figure 7. (a)Voltage across the inductor (b) Current through the inductor (c) Output voltage across the load (d) Output current through the load during buck mode.

2.2.1.3. Bidirectional Mode (Buck)

Consider an input voltage of $E_{\text{in}} = -160$ V for bidirectional operation as shown in Fig. 8(a). S_{W4}, the switching signal, was provided with a duty ratio (d_4) = 34%. The voltage across the inductor $E_L = 81.65$ V, which was shown in Fig. 8(b). The current flows through the inductor while discharging and charging was from -40.9 A to -41.79 A, as shown in Fig. 8(c).

The output voltage will be the sum of the voltage across both resistors, as shown in Fig. 8(d) and Fig. 8(e). (i.e., $E_{o1} = 40.8$ V, $E_{o2} = 40.8$ V, $E_o = 81.61$ V (i.e., $(E_{o1} + E_{o2})$), and the output current was $I_o = 81.61$ A, as shown in Fig. 8(f) and Fig. 8(g).)

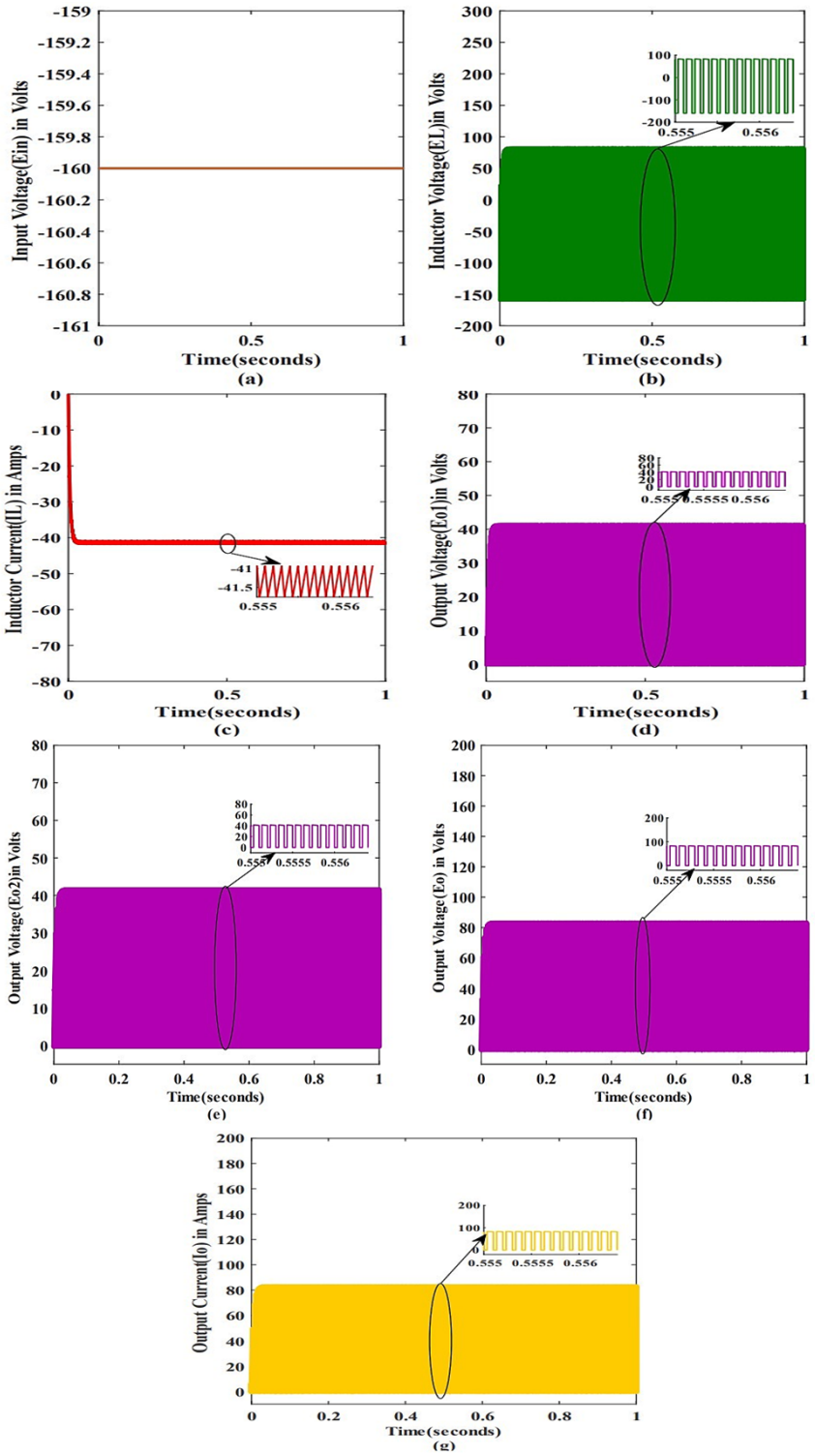

Figure 8. (a)Ein as Input voltage. (b) Voltage across the inductor. (c) Current through the inductor. (d) Output voltage across the load (Eo1). (e) Output voltage across the load (Eo2). (f) Output voltage across the load (Eo). (g) Output current through the load. (Io) during bidirectional mode.

2.3. Closed loop simulation

The main objective of closed loop simulation was to generate the appropriate duty ratios d_1, d_2 and d_3, for the switches S_{W1}, S_{W2}, and S_{W3} in order to obtain the output voltage and current with minimum error values when compared with open loop simulation. For simulation study, the time domain specification was considered as performance analysis parameters for both open and closed loop simulation. The trial and error method was adopted to generate the K_P and K_I values required for the PI controller.

2.2.2.1. Closed loop control strategy

Dual-input DC/DC converter was used to combine the energy sources which have distinct (V-I) characteristics. Proportional-Integral controller was used to regulate the output voltage and current by controlling the duty cycle of the switches. The comparator compares E_{ref} with E_o and generates an error signal, which was provided to PI Controller-I (voltage controlled-PI). PI Controller-I output was compared with I_o and the error signal was provided to another PI controller-II (current controlled-PI), which generates an error signal. The error signal was provided to three pulse generator modules in order to generate the duty ratio for the corresponding switches. A PI-based Dual-Input DC/DC converter was shown in Fig. 9.

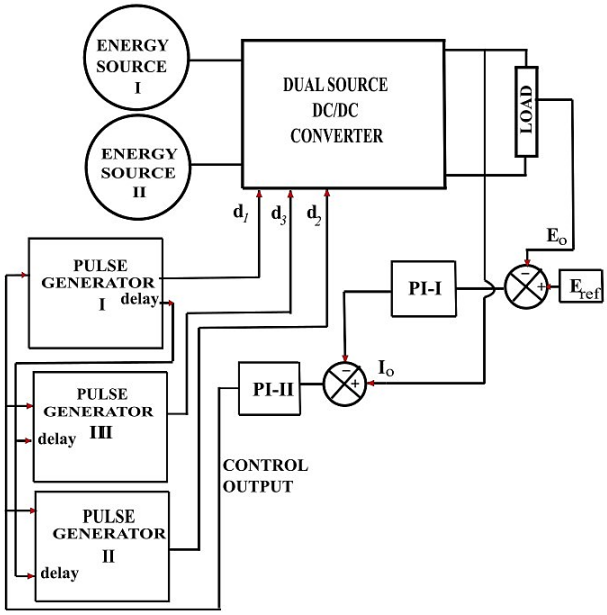

Figure 9. Closed loop schematic of dual input DC/DC Converter.

2.2.2.2. PI-Boost Mode

The gain values chosen for PI Controller-I are as follows: $K_p = 0.01$ and $K_I = 1.9$, and the value chosen for PI Controller-II was $K_p = 0$ and $K_I = 0.0001$. The inductor was charged to a voltage of 48 V for a particular time period (i.e., $E_1 - E_o$), and then the inductor was further charged to 84 V (i.e., $E_1 + E_2 - E_o$). The inductor was finally charged to 36 V (i.e., $E_2 - E_o$) and was eventually discharged to $(-E_o)$, i.e., -160 V.

The inductor current undergoes a sequence of charging and discharging from 58.65 A to 57.98 A, as shown in Fig. 10(a) and Fig. 10(b). The voltage $(-E_o)$ and current $(-I_o)$ across the load resistance (output resistance) were -160 V and -16 A, as shown in Fig. 10(c) and Fig. 10(d).

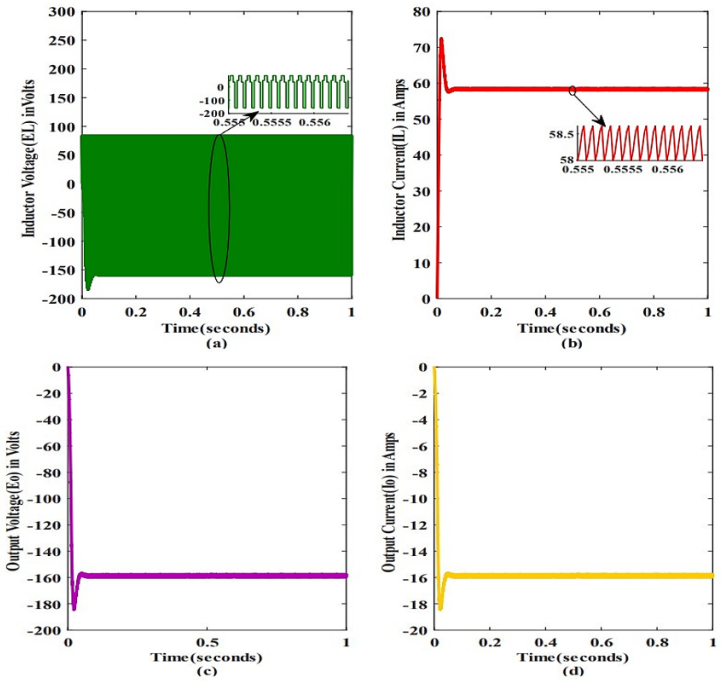

Figure 10. (a)Voltage across the inductor (b) Current through the inductor (c) Output voltage across the load (d) Output current through the load during PI-boost mode.

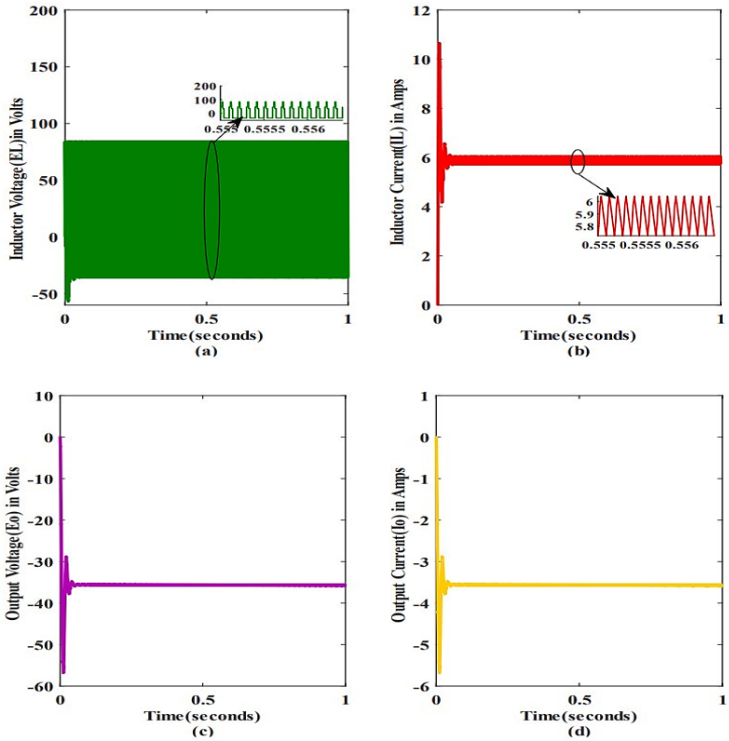

Figure 11. (a)Voltage across the inductor (b) Current through the inductor (c) Output voltage across the load (d) Output current through the load during PI-buck mode.

2.2.2.3. PI-Buck Mode

The gain values provided to the PI Controller-I were $K_P = 1$ and $K_I = 0.01$, and the value for PI Controller-II was chosen as $K_P = 0$ and $K_I = 0.001$. The inductor was charged to a voltage of 48 V (i.e., $E_1 - E_o$), 36 V (i.e., $E_2 - E_o$), and 84 V (i.e., $E_1 + E_2 - E_o$) for a specific time period. Lastly, the inductor was discharged to a voltage of -35 V (i.e., $-E_o$) for the rest of the time interval.

The inductor was charged to a current of 6.05 A and discharged to a current of 5.725 A, as shown in Fig. 11(a) and Fig. 11(b). Output voltage and output current across the load resistance were -35 V and -3.5 A, as shown in Fig. 11(c) and Fig. 11(d).

3. Performance Analysis of the Converter

Dual-input DC/DC converter's performance was validated by considering certain parameters such as average output power, efficiency, and output voltage. The boost mode duty cycle with input voltage (E_1) of 48 V and the input voltage (E_2) of 36 V was taken into account for analysis.

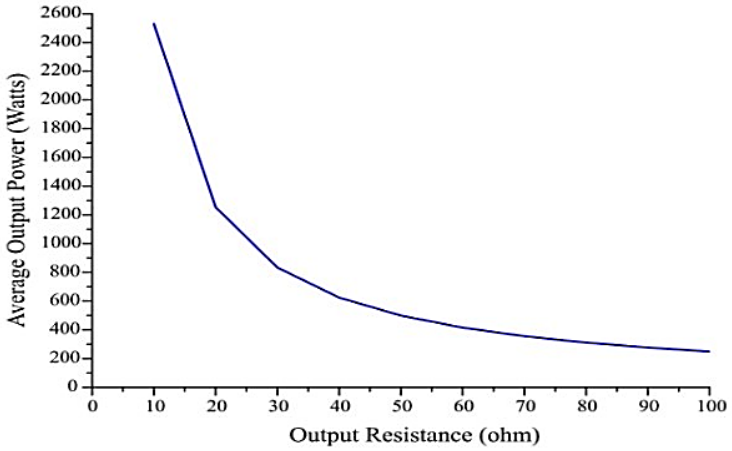

Figure 12. Average output power of DIC over change in load resistance.

From Figure Figure 12. it was noticed that the converter can yield more average output power with respect to change in load resistance.

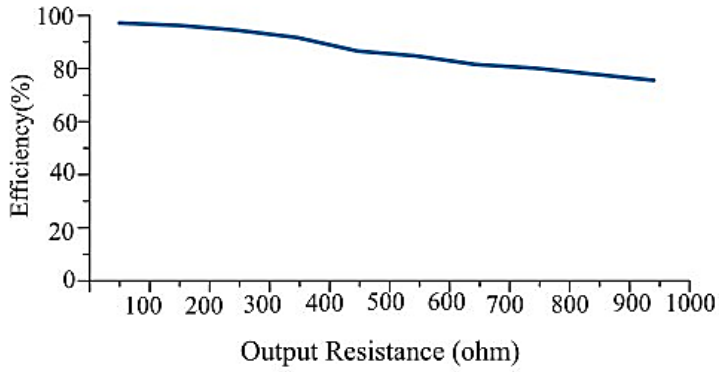

Figure 13. Efficiency of DIC over change in load resistance.

From the graph it was observed that the increase in load resistance will decrease the converter efficiency as shown in Figure 13.

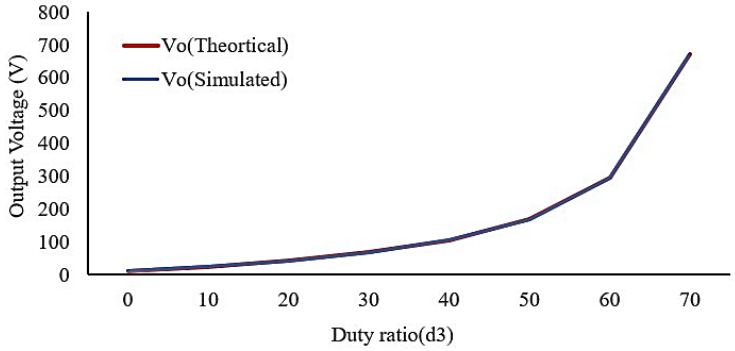

Figure 14. Output voltage across the load resistance Vs duty cycle (d_3).

The output voltage across the load resistance was correlated with duty cycle and it was shown in Figure 14. In order to obtain the above graph, certain parameters are taken into consideration such as the input voltage (E_1) as 48 V, input voltage (E_2) as 36 V, and the duty cycle provided to the corresponding switches are $d_1 = 10\%$, $d_2 = 10\%$, and $d_3 = 0\%$ to 70%.

The DIC provides a high output voltage of 670 V, efficiency of 96%, and high average output power of 2560 W when compared with other existing converters ranging from an output voltage of 150 to 300 V, efficiency of 78 to 95%, and an average output power of 200 W to 1000 W as discussed by Athikkal et al.

3.1. Results and Discussion

Time domain specifications such as rise time (t_r), peak time (t_p), maximum peak overshoot (M_p), settling time (t_s), and steady state error (e_{ss}) were measured in both open loop and closed loop in order to evaluate the performance of the converter. The time domain analysis of the converter was shown in Table 2.

Table 2. Time domain analysis of the converter

Open loop	t_r (ms)	t_p (ms)	M_p (V)	t_s (ms)	e_{ss} (V)
Boost operation	15.6	23.5	8.5	75.03	1.5
Buck operation	5.52	9	12.1	76.31	0.3
Closed loop	t_r (ms)	t_p (ms)	M_p (V)	t_s (ms)	e_{ss} (V)
PI-Boost operation	15	21.8	24	65.29	0
PI-Buck operation	3.29	8.5	21	70.75	0

Manikandan et al. has proposed an interleaved boost converter for Permanent Magnet DC (PMDC) motor and assessed the time domain parameters for various speed ranges, namely 1000, 950, and 900 rpm. For 1000 rpm, they have achieved a $t_r = 1.74$ sec, $t_p = 2.10$ sec, $t_s = 2.15$ sec, and $e_{ss} = 1.6$. For 950 rpm, they have achieved a $t_r = 1.77$ sec, $t_p = 2.30$ sec, $t_s = 2.75$ sec, and $e_{ss} = 1.8$. For 900 rpm, they have achieved a $t_r = 1.79$ sec, $t_p = 2.48$ sec, $t_s = 2.86$ sec, and $e_{ss} = 1.9$. When compared with the above results, the proposed results listed in Table 2 indicate that the closed-loop simulation of the dual-input DC/DC converter provides a reduced $t_r = 15$ ms, $t_p = 21.8$ ms, $t_s = 65.29$ ms, and $e_{ss} = 0$ for PI Boost Mode, and for PI-Buck mode, $t_r = 3.29$ ms, $t_p = 8.5$ ms, $t_s = 70.75$ ms, and $e_{ss} = 0$, while increasing the Maximum peak overshoot (M_p) in both modes of operation. Hence, the converter in closed-loop simulation enhances the speed of response and also provides an accurate estimation of time domain parameters.

4. Conclusions

A detailed analysis of dual input DC/DC converter such as topological architecture, mode of operation, output equation, steady-state waveform, design parameters, and an open and closed loop simulation was described in this article. An effort was made to improve the performance of the converter by implementing a closed-loop control strategy. The various electrical parameters and time-domain specification are taken into account in order to show the workability of the converter. In terms of electrical parameters, the converter provides an average output power of 250 W to 2560 W, the efficiency of the converter will vary from 89% to 96%. An increase in output voltage of 10 V to 670 V for change in duty cycle (d3).During PI - Boost mode of operation the converters rise time is reduced from 15.6 to 15 ms, peak time is reduced from 23.5 ms to 21.8 ms, settling time is reduced from 75.03 to 65.29 ms and achieved a steady state error of zero from 1.5, then for PI- Buck mode of operation the converter rise time is reduced from 5.52 to 3.29 ms, peak time from 9 to 8.5 ms, settling time from 76.31 to 70.75 ms and a steady state error is reduced from 0.3 to 0. From the results, the closed loop control of converter provides a simultaneous power delivery with increased efficiency, high average output power, wide control range of output voltage and an accurate estimation of time domain parameters. The drawback encountered in the present converter under closed loop simulation is increase in maximum peak overshoot (% Mp) which need to resolved and a Forthcoming research work will focus on developing an experimental prototype of the converter.

Funding: This research received no external funding.

Author contributions: Conceptualization, Methodology, Investigation, and Writing an original draft, Y.H.V.; Review and Supervision, S.K.L.

Disclosure statement: The authors declare no conflict of interest.

References

[1] Sivaprasad Athikkal, Gangavarapu Guru Kumar, Kumaravel Sundaramoorthy, and Ashok Sankar. A non-isolated bridge-type dc–dc converter for hybrid energy source integration. *IEEE Transactions on Industry Applications*, 55(4):4033–4043, May 2019.

[2] Jeba Singh Oliver, Prince Winston David, Praveen Kumar Balachandran, and Lucian Mihet-Popa. Analysis of grid-interactive pv-fed bldc pump using optimized mppt in dc–dc converters. *Sustainability*, 14(12):7205, June 2022.

[3] Sivaprasad Athikkal, Kumaravel Sundaramoorthy, and Ashok Sankar. Design, fabrication and performance analysis of a two input—single output dc-dc converter. *Energies*, 10(9):1410, September 2017.

[4] Mohammad Reza Banaei, Hossein Ardi, Rana Alizadeh, and Amir Farakhor. Non-isolated multi-input–single-output dc/dc converter for photovoltaic power generation systems. *IET Power Electronics*, 7(11):2806–2816, August 2014.

[5] R. Amaleswari and M. Prabhakar. Non-isolated multi-input dc-dc converter with current sharing mechanism. *International Journal of Electronics*, 108(2):237–263, June 2020.

[6] Lalit Kumar and Shailendra Jain. Multiple-input dc/dc converter topology for hybrid energy system. *IET Power Electronics*, 6(8):1483–1501, August 2013.

[7] Koganti Srilakshmi, N Yashaswini, Sravanthy Gaddameedhi, Ramprasad Vangalapudi, Praveen Kumar Balachandran, Surender Reddy Salkuti, and Fayaz Basha. Development of ai-controller for solar /battery fed h-bridge cascaded multilevel converter upqc under different loading conditions. *International Journal of Renewable Energy Research (IJRER)*, 14(2):403–417, 2024.

[8] Sivaprasad Athikkal, Kumaravel Sundaramoorthy, and Ashok Sankar. A modified dual input dc-dc converter for hybrid energy application. *International Journal of Power Electronics and Drive Systems/International Journal of Electrical and Computer Engineering*, 8(1):81, March 2017.

[9] Sivaprasad Athikkal, Kumaravel Sundaramoorthy, and Ashok Sankar. Development and performance analysis of dual-input dc–dc converters for dc microgrid application. *IEEJ Transactions on Electrical and Electronic Engineering*, 13(7):1034–1043, March 2018.

[10] S. Kumaravel, G. Guru Kumar, Kuruva Veeranna, and V. Karthikeyan. Novel non-isolated modified interleaved dc-dc converter to integrate ultracapacitor and battery sources for electric vehicle application. *2018 20th National Power Systems Conference (NPSC)*, page 1–6, December 2018.

[11] Lalit Kumar and Shailendra Jain. A novel dual input dc/dc converter topology. *2012 IEEE International Conference on Power Electronics, Drives and Energy Systems (PEDES)*, page 1–6, December 2012.

[12] Sivaprasad Athikkal, Gangavarapu Guru Kumar, Kumaravel Sundaramoorthy, and Ashok Sankar. Performance analysis of novel bridge type dual input dc-dc converters. *IEEE Access*, 5:15340–15353, January 2017.

[13] Sivaprasad Athikkal, Gangavarapu Guru Kumar, Kumaravel Sundaramoorthy, and Ashok Sankar. Performance analysis of a positive output voltage dual input dc–dc converter for hybrid energy application. *Journal of Circuits Systems and Computers*, 27(10):1850159, January 2018.

[14] Kushal KANHAV and Madhuri CHAUDHARI. Experimental realization of a multi-input buckboost DC-DC converter. *TURKISH JOURNAL OF ELECTRICAL ENGINEERING COMPUTER SCIENCES*, 26(3), May 2018.

[15] Hitendra Singh Thakur and Ram Narayan Patel. Design and development of dual input dc–dc converter for hybrid energy system. *Journal of Circuits Systems and Computers*, 28(07):1950109, July 2018.

[16] Zubair Rehman, Ibrahim Al-Bahadly, and Subhas Mukhopadhyay. Multi-input dc–dc converters in renewable energy applications – an overview. *Renewable and Sustainable Energy Reviews*, 41:521–539, September 2014.

[17] Ali Deihimi, Mir Esmaeel Seyed Mahmoodieh, and Reza Iravani. A new multi-input step-up dc–dc converter for hybrid energy systems. *Electric Power Systems Research*, 149:111–124, April 2017.

[18] Koganti Srilakshmi, Dheeraj Sundaragiri, Sravanthy Gaddameedhi, Ramprasad Vangalapudi, Praveen Kumar Balachandran, Ilhami Colak, and Shitharath Selvarajan. Simulation of grid/standalone solar energy supplied reduced switch converter with optimal fuzzy logic controller using golden ballalgorithm. *Frontiers in Energy Research*, 12, March 2024.

[19] S. Khosrogorji, M. Ahmadian, H. Torkaman, and S. Soori. Multi-input dc/dc converters in connection with distributed generation units – a review. *Renewable and Sustainable Energy Reviews*, 66:360–379, 2016.

[20] Azuka Affam, Yonis M. Buswig, Al-Khalid Bin Hj Othman, Norhuzaimin Bin Julai, and Ohirul Qays. A review of multiple input dc-dc converter topologies linked with hybrid electric vehicles and renewable energy systems. *Renewable and Sustainable Energy Reviews*, 135:110186, August 2020.

[21] Gangavarapu Guru Kumar, Kumaravel Sundaramoorthy, Sivaprasad Athikkal, and Venkitusamy Karthikeyan. Dual input superboost dc–dc converter for solar powered electric vehicle. *IET Power Electronics*, 12(9):2276–2284, May 2019.

[22] K. T. Maheswari, C. Kumar, Praveen Kumar Balachandran, and Tomonobu Senjyu. Modeling and analysis of the lc filter-integrated quasi z-source indirect matrix converter for the wind energy conversion system. *Frontiers in Energy Research*, 11, August 2023.

[23] Liang Xian, Gucheng Wang, and Youyi Wang. Implementation and control of a double-input dc/dc converter for pemfc/battery hybrid power supply. *2012 7th IEEE Conference on Industrial Electronics and Applications (ICIEA)*, July 2012.

[24] Lenin Prakash, Arutchelvi Meenakshi Sundaram, and Stanley Jesudaiyan. A simplified time-domain design and implementation of cascaded pi-sliding mode controller for dc–dc converters used in off-grid photovoltaic applications with field test results. *Sadhana*, 42(5):687–699, March 2017.

[25] C. T. Manikandan, G. T. Sundarrajan, V. Gokula Krishnan, and Isaac Ofori. Performance analysis of two-loop interleaved boost converter fed pmdc-motor system using flc. *Mathematical Problems in Engineering*, 2022:1–12, August 2022.

[26] Belqasem Aljafari, Praveen Kumar Balachandran, Devakirubakaran Samithas, and Sudhakar Babu Thanikanti. Solar photovoltaic converter controller using opposition-based reinforcement learning with butterfly optimization algorithm under partial shading conditions. *Environmental Science and Pollution Research*, 30(28):72617–72640, May 2023.

[27] Sudhakar Babu Thanikanti, Praveen Kumar B, Devakirubakaran S, Belqasem Aljafari, and Ilhami Colak. A dynamic mismatch loss mitigation algorithm with dual input dual output converter for solar pv systems. *Solar Energy Materials and Solar Cells*, 251:112163, December 2022.